Chin. J. Astron. Astrophys. Vol. 8 (2008), No. 1, 50–62
(*http://www.chjaa.org*)

Chinese Journal of
Astronomy and
Astrophysics

Geometry of Broad Line Regions of Active Galactic Nuclei

Xiao-Rong Lü

[1] Key Laboratory for Particle Astrophysics, Institute of High Energy Physics, Chinese Academy of Sciences, Beijing 100049; *rrlv2003@yahoo.com.cn*
[2] Graduate School of Chinese Academy of Sciences, Beijing 100049

Received 2007 February 9; accepted 2007 June 1

Abstract It has long remained an open question as to the geometry of the broad line region (BLR) in active galactic nuclei (AGNs). The reverberation mapping technique which measures the response of the broad emission lines to the ionizing continuum, when combined with multiwavelength continuum fitted by sophisticated accretion disks, provides a way of probing the BLR geometry. We analyze a sample of 35 AGNs, which have been monitored by the reverberation mapping campaign. In view of energy budget, the reverberation-based BH masses are found to be in agreement with those obtained by accretion disk models in two thirds of the present sample while the reverberation mapping methods underestimate the BH masses in about one third of objects, as also suggested by Collin et al. in a recent work. We point out that there are obviously two kinds of BLR geometry, which are strongly dependent on the Eddington ratio, and separated by the value $L_{\rm Bol}/L_{\rm Edd} \sim 0.1$. These results prefer a scenario of the disk and wind configuration of the BLR and identify the Eddington ratio as the physical driver regulating the wind in the BLR.

Key words: accretion, accretion disks — galaxies: active — galaxies: Seyfert — quasars: general

1 INTRODUCTION

It is widely accepted that active galactic nuclei (AGNs) are powered by supermassive black holes (SMBHs). The broad line region (BLR), close to the innermost part of the central engine provides an important clue to the understanding of the physical processes in the vicinity of the SMBHs. The so-called reverberation mapping campaign was carried out to determine the SMBH mass in AGNs assuming that the potential of the SMBHs dominates in the BLR (Blandford & McKee 1982; Peterson 1993; Wandel et al. 1999; Kaspi et al. 2000). With the distance to the SMBH determined by the echo of the emission line to the continuum, the black hole mass is then given by

$$M_\bullet = f\frac{c\Delta\tau\, V_{\rm H\beta}^2}{G}, \tag{1}$$

where $\Delta\tau$ is the time delay between the ionizing continuum and the Balmer emission line Hβ, G the gravity constant, c the light speed and $V_{\rm H\beta}$ the full width at half-maximum (FWHM) of Hβ. Here f is a geometric factor depending on the structure, kinematics and inclination of the BLR (Krolik 2001). In principle $\Delta\tau$ and $V_{\rm H\beta}$ can be measured accurately enough, but the factor f remains open so far.

To understand the geometry of BLR, therefore, is of critical importance. One attractive idea proposed earlier is that the BLR has an accretion disk or disk-like structure that is dominated by rotational motion (Perez et al. 1988; Chen & Halpern 1989) since the accretion disk is the most likely configuration established in AGNs. This simple disk model, however, was set back by the finding that it is single-peaked

emission lines, rather than double-peaked ones predicted by disk geometry that are mostly observed in AGNs (Eracleous & Halpern 1994; Strateva et al. 2003). Murray & Chiang (1995,1997) then introduced wind emerging from the disk to resolve this conflict. According to the disk-wind model, single-peaked lines could be produced if there is a large radial velocity shear so that photons can escape along directions with small line-of-sight projected velocity. Various models based on a flattened disk with associated winds in the BLR have been intensively explored (Dumont & Collin-Suffrin 1990; Sulentic et al. 1998; Eracleous & Halpern 2003; Shapovalova et al. 2004; Popović et al. 2001, 2003). On the other hand, profiles of broad emission lines characterized by complicated substructures give an indication that the BLR is likely to be composed of several emission regions with significantly different physical properties as well as kinematics of the photoionized gas (Romano et al. 1996; Zhang & Wu 2002). Popović (2003) proposed, for the BLR geometry, a two-component model consisting of a disk-like region and a spherical region, with the latter originating from such disk associated mechanism as wind. However, the two-component model does not give strong constraints on the BLR geometry because of too many free parameters involved, leaving possible other configurations like the disk+jet. Recently, Sulentic et al. (2000) suggested that there may exist different BLR geometries, which is tightly related to the variety of AGNs (see also Marziani et al. 2003; Collin et al. 2006). The different BLR geometries and its implications are also explored in a more recent work (Lamastra et al. 2006).

We make an attempt to investigate the geometry of the BLR through combining the reverberation mapping technique with the method based on the multiwavelength continuum fittings using an accretion disk model considering vertical disk structure to determine the black hole (BH) mass. By comparing these two independent mass estimators, the deduced geometric factor sets up strong constraints on the structure of the broad line region.

We make an attempt to investigate the geometry of the BLR through comparing two methods of determining the mass of the black hole (BH): by the reverberation mapping technique and by multiwavelength continuum fitting with an accretion disk model that includes vertical disk structure. By comparing these two independent mass estimators, the deduced geometric factor sets up strong constraints on the structure of the BLR. In Section 2 we introduce our sample and the data reduction techniques, and present the method of multiwavelength continuum fitting. In Section 3, the results are analyzed. We give a discussion in Section 4, and finally conclusions are presented in Section 5. We set the Hubble constant at $H_0 = 75\ \mathrm{km\ s^{-1}\ Mpc^{-1}}$ and deceleration factor at $q_0 = 0.5$ throughout this paper.

2 SAMPLE AND METHOD

2.1 Sample and Data Reduction

We assembled all the 35 objects from Peterson et al. (2004) with their black hole masses measured by the reverberation mapping technique. At the present time, the reverberation data have been published only for ten Seyfert galaxies in AGN watch database. We obtained the continuum data of nine objects in the present sample from the website *(http://www.astronomy.ohio-state.edu/∼agnwatch/)*. The data of the PG quasars were downloaded from *http://wise-obs.tau.ac.il/∼shai/PG/*. For 11 objects without available reverberation data from either websites, we adopted the data of L_{5100} (the luminosity at 5100Å) given by Peterson et al. (2004), these are PG 0003, Mrk 79, Mrk 110, Mrk 590, Mrk 817, NGC 3227, NGC 3516, NGC 4593, 3C120, Akn 120 and IC 4329A. These objects have usually been observed for many times, then the averaged spectra were taken. We also collected the multiwavelength continuum from the literature and calculated their averaged spectra for the fitting program. Most of the data are taken from Neugebauer et al. (1986,1987) and NASA/IPAC Extragalactic Database. Generally, the Seyfert galaxies have much more violent variabilities than the PG quasars. Since the continuum data are *not* simultaneous, we give the reverberation mapping data the top priority when available from the internet. We estimated the bolometric luminosity with $L_{\rm Bol} = 9L_{5100}$ from the reverberation data (Peterson et al. 2004), and found all objects satisfy $L_{\rm Bol}/L_{\rm Edd} < 0.3$, as required by the standard accretion disk model (Laor & Netzer 1989). For most sources in the sample (28/35), the luminosity satisfies $L(B) \geqslant 10^{43.5}\mathrm{erg\ s^{-1}}$ to avoid significant star-light contamination from underlying galaxy; the other, lower-luminosity sources (7/35) are discussed in Section 3. The observed data are corrected for galactic extinction according to the extinction law of Seaton (1979). The intrinsic extinction to quasars are thought to be small, with the upper limit value of continuum reddening of $E(B-V) \sim 0.05$ (Sun & Malkan 1989; Laor 1990). Besides, the Balmer continuum and blended Fe II emission

would also contribute to the overall multiwavelength spectrum from IR to UV. The Balmer continuum mainly affects the fitting from 3200 to 3700 Å (in rest frame), and the blended Fe II emission from 2400 to 2700 Å. The contaminations from these two components are estimated to be only 17 per cent of the near-ultraviolet fluxes (Malkan 1988), and in fact, the possible influences on the fitted disk parameters are negligible (Sun & Malkan 1989).

The X-ray data of sources are from available EPIC observations in the *XMM*-Newton Science Archive (XSA). The sample and data are given in Table 1, including the observation dates, revolution numbers and ID. The Observation Data Files (ODFs) from the EPIC instruments are processed according to the *XMM-Newton* Science Analysis System (SAS v6.4.0) and the most updated calibration files. Source spectra were extracted from circular regions with a radius of $40''$, and backgrounds were selected in an source-free circular of the equal radius close to the sources on the same CCD. According to the current calibration uncertainties we perform the spectral analysis in the 0.3–12 keV bands for the pn cameras. The source spectra were grouped such that each spectral bin contains at least 35 counts so that the χ^2 statistics would be applicable. The fitting was done using XSPEC v11.2 (Arnaud 1996).

2.2 Accretion Disk Model with Vertical Structure

The observed big blue bumps are explained by energy release of accretion onto the black hole. The detailed description of the present accretion disk model can be found in Dörrer et al. (1996), here we only recall its main features: 1) A standard accretion disk (Shakura & Sunyaev 1973), namely the structure in radial direction is decoupled from the vertical and the gas rotates with a Keplerian velocity and vertical equilibrium holds at any radius; 2) The chemical composition is pure hydrogen and fully ionized. The radiation mechanisms are free-free emission and Comptonization, neglecting bound-bound absorption and bound-free absorption. 3) Viscosity $\alpha-$description. Most of the difficulties in the vertical structure are due to the viscosity in the different layers. The widely used $\alpha-$description of viscosity should be specified for different layers. Dörrer et al. (1996) assumed that the energy is produced by the turbulence, with velocity given by

$$V_{\rm turb} = \frac{\tau + \sqrt{\beta}}{1+\tau} c_s, \tag{2}$$

with sound speed c_s, optical depth $\tau = \int_z^H \kappa_{\rm F} \rho dz$ and pressure ratio $\beta = P_{\rm gas}/(P_{\rm gas} + P_{\rm rad})$. The phenomenological formula of the viscosity description takes into account the loss of radiative energy by a turbulence elements in an optically thin regime. This model presents a self-consistent calculation of the vertical structure and emergent spectrum of an accretion disk around a massive black hole. The emergent spectrum has been corrected by the general relativistic effects using the ray tracing method.

We calculate a spectral grid for black hole masses $\log m_\bullet = 6.0 - 9.7$, accretion rates $\dot{m} = 0.05, 0.1, 0.2, 0.3$, spins $a = 0.0, 0.3, 0.6, 0.7, 0.8, 0.998$, and cosines of the viewing angle $\cos\Theta = 0.05, 0.25, 0.50, 0.75, 1.0$, where $m_\bullet = M_\bullet/M_\odot$ and $\dot{m} = \eta c^2 \dot{M}/L_{\rm Edd}$, η is mass-to-energy conversion efficiency, which is dependent on the spin parameter in the present disk model. We thus have $38 \times 4 \times 6 \times 5 = 4560$ grid files for linear interpolations. Following Dörrer et al. (1996), we fix the viscosity parameter $\alpha = 1/3$ for all the models. We tested the grid accuracy with finer grids, and found the accuracy of the interpolation to be better than 95%, which was sufficient for our fittings.

2.3 Fitting Procedure

We model the continuum from the infrared to hard X-ray by three components: 1) The contribution from the reprocessing of the dusty torus,

$$F_{\rm IR}(\nu) = F_1 \nu^{-\beta_1} \exp\left(-\nu/\nu_{\rm c}^{\rm IR}\right), \tag{3}$$

where F_1 is the normalization constant, β_1 the index of the power law, and $\nu_{\rm c}^{\rm IR}$ the cutoff frequency. Considering the complication in the near infrared emission (Kishimoto et al. 2005), the cutoff frequency is not solely determined by the thermal temperature of the dust, and we assume the simple power law plus an exponential cutoff component to roughly represent a continuum component different from the accretion disk. 2) The X-ray spectrum can be fitted by a sum of a black body and a power law (2–10 keV) from the

Table 1 Observational Journals of the Sample

Name	z	OUV Ref.	Obs. Date	Rev.	Obs-ID	$N_{\rm H}^{\rm Gal}$
PG 0003+199	0.026	1, 4	2000-12-25	0192	0101040701	3.70^a
PG 0026+129	0.142	1, 2	–	–	–	–
PG 0052+251	0.155	1, 2	2005-06-26	1016	0301450401	4.50^b
PG 0804+761	0.100	1, 2	–	–	–	–
PG 0844+349	0.064	1, 2	2000-11-04	0166	0103660201	3.32^c
PG 0953+414	0.234	1, 2	2001-11-22	0358	0111290201	1.12^c
PG 1211+143	0.081	1, 2	2001-06-15	0270	0112610101	2.76^c
PG 1226+023	0.158	1, 2	2004-06-30	0835	0136550801	2.00^d
PG 1229+204	0.063	1, 2	2005-07-09	1022	0301450201	2.58^b
PG 1307+085	0.155	1, 2	2002-06-13	0460	0110950401	2.11^b
PG 1411+442	0.089	1, 2	2002-07-10	0473	0103660101	1.05^c
PG 1426+015	0.086	1, 2	2000-07-28	0116	0102040501	2.64^b
PG 1613+658	0.129	1, 2	2001-04-13	0246	0102040601	2.66^b
PG 1617+175	0.112	1, 2	–	–	–	–
PG 1700+518	0.292	1, 2	–	–	–	–
PG 2130+099	0.063	1, 2	2003-05-16	0629	0150470701	4.20^b
Mrk 79	0.022	1, 4	2001-04-26	0253	0103862101	5.89^b
Mrk 110	0.035	1, 4	2004-11-15	0904	0201130501	1.21^a
Mrk 279	0.031	1, 3	–	–	–	–
Mrk 509	0.034	1, 3	2001-04-20	0250	0130720201	4.44^a
Mrk 590	0.026	1, 4	2002-01-01	0378	0109130301	3.07^a
Mrk 817	0.032	1, 4	–	–	–	–
NGC 3227	0.004	1, 4	2000-11-28	0178	0101040301	2.07^a
NGC 3516	0.009	1, 4	2001-04-10	0245	0107460601	2.94^a
NGC 3783	0.009	1, 3	2001-12-19	0372	0112210501	9.59^a
NGC 4051	0.002	1, 3	2002-11-22	0541	0157560101	1.31^b
NGC 4151	0.003	1, 3	2000-12-22	0190	0112830201	2.17^a
NGC 4593	0.009	1, 4	2002-06-23	0465	0059830101	1.97^b
NGC 5548	0.017	1, 3	2000-12-24	0191	0109960101	1.61^a
NGC 7469	0.016	1, 3	2004-12-03	0913	0207090201	4.82^b
3C 120	0.033	1, 4	2002-09-06	0502	0109131101	12.32^b
3C390.3	0.056	1, 3	2004-10-08	0885	0203720201	3.68^a
Akn 120	0.032	1, 4	2003-08-24	0679	0147190101	15.10^d
IC 4329A	0.016	1, 4	–	–	–	–
Fairall 9	0.047	1, 3	2000-07-05	0105	0101040201	5.00^d

NOTES/REFERENCES:– (1) source name; (2) redshift; (3) references for optical data; (4) observation date (yyyy-mm-dd) with *XMM-Newton*; (5) orbit revolution number; (6) Observation ID; (7) Galactic absorption $N_{\rm H}^{\rm Gal}$ values in 10^{20} cm^{-2}: *a*-Murphy et al. (1996); *b*-Elvis et al. (1989); *c*-Lockman & Savage (1995); *d*-by fittings.
Ref: 1: from NASA/IPAC Extragalactic Database (NED), especially from Neugebauer et al. (1987, 1986); 2: from Kaspi et al. (2000); 3: from AGN Watch; 4: from Peterson et al. (2004).

hot corona (Brocksopp et al. 2006):

$$F_{\rm X}(\nu) = \left(B_\nu(T) + F_2\nu^{-\beta_2}\right)\exp\left(-N_{\rm H}\sigma_\nu\right), \tag{4}$$

where $B_\nu(T)$ is the Planck function, $N_{\rm H}$ the hydrogen column density, and σ_ν the absorption section. Actually, the soft X-ray spectrum, the so-called *soft excess* below 2–3 keV (Arnaud et al. 1985; Turner & Pounds 1989) is so complicated that none of simple models can satisfy all the AGNs, and some other models have been tried: e.g., a broken power law, or a sum of a multi-color black body and a power law, etc., with additional ionized absorption/absorption edge components whenever appropriate according to the *F-test* criterion at a significance level $\geq 95\%$ (Porquet et al. 2004; Piconcelli et al. 2005; Crummy et al. 2006). Note that, here, we use the X-ray spectra mainly for constraints on the accretion rates. 3) Emergent spectrum from the accretion disk,

$$F_{\rm disk}(\nu) = \mathcal{F}(\dot{m}, M_\bullet, a, \Theta)\,. \tag{5}$$

The best fit is obtained by minimizing when $\chi^2 = \sum_{i=1}^{N} \left[F_0^i(\nu) - F_{\rm IR}(\nu) - F_{\rm disk}(\nu)\right]^2 / \sigma_i^2$, where σ_i is the error bar of $F_0^i(\nu)$, the observed flux at frequency ν, N the total number of data-points from the optical to the ultraviolet. The initial fitting was made by directly inserting the reverberation-based mass of the black hole into the disk model. The accretion rate is constrained by the X-ray spectrum. The spin of the black hole is set either at $a = 0.0$ (i.e. Sch. BH) or at $a = 0.998$ (i.e. Kerr BH). The initial fitting provides a unique way of finding the best fitting, also a most strong constraint on the reverberation mapping technique. We then relax all the parameters in the disk models to fit the observed data. The fitting converges when minimum χ^2 is reached. For some highly variable sources, however, we actually require the disk model passing through most of the spectral points when χ^2 becomes meaningless. Based on $\chi^2_{\rm min}$, the error bars are given from $\Delta\chi^2_{\rm min} = 2.7$ at a 90% level of significance.

3 RESULTS

Plots of fittings for 35 objects in the present sample show the multiwavelength continuum and the fitting results (see *http:// www.chjaa.org / 2008_8_1p50*). We fit the multiwavelength continuum with the accretion disk model with vertical structure, for Schwarzschild and Kerr black holes, respectively. First, we consider the case in which the BH mass is fixed at the value given by the reverberation-mapping to test for energy budget. Then we obtained the BH mass with the full accretion disk model. The fitting results are shown in Tables 2 and 3, respectively. In Table 4 we list the models applied to the X-ray bands and the resulting values of the spectral parameters.

The X-ray emission (0.3–12 keV) of AGNs contains significant features of soft excess (below 2–3 keV) and complex absorption. The soft excess has been found in all the sources in the present sample (Crummy et al. 2006). The warm absorption features are present in 35% of the QSOs spectra, and are also found in a low-redshift PG quasars sample (Porquet et al. 2004). Seyfert galaxies generally exhibit more complex emission and absorption features, that could be fitted using multi-ionized absorption components (ABSORI in XSPEC). Due to the complexity of the soft excess, several approximate parameterization models have been used to reproduce the spectra of the present sample. The inferred fitting parameters found, such as the roughly constant temperature of blackbody $kT \sim 0.1 - 0.2$ keV, and the photon index $1.5 < \Gamma < 2.9$, are consistent with the previous fitting results (e.g. Crummy et al. 2006; Porquet et al. 2004). Although these models satisfactorily fitted the majority of the spectra ($\chi^2_\nu < 1.2$), a physical explanation of the origin of the soft excess requires more detailed theory (e.g. Ross & Fabian 2005), which is outside the scope of this paper. Note that we use the X-ray spectra mainly to constrain the accretion rate parameters in all the above fitting procedures. The X-ray flux would provide an upper limit to the accretion rate, then the accretion disk models will not overestimate the mass, thus providing a test of the reverberation-based mass. From these spectral fittings, we find:

1) Better fits to the multiwavelength continuum are generally obtained for disk models containing a Kerr BH than a Schwarzschild BH. This result may have a bearing on the fact that most BHs have fast spins, as evidenced by the very broad profile of the iron Kα line in MCG-6-30-15 (Fabian et al. 2002), corroborated by the recent simulation results (Volonteri et al. 2005). Further considerations on the spins of BHs are beyond the scope of the present paper, so we shall consider only the Kerr BH mass obtained by the AD model below.

II) The fits with the reverberation-based mass are significantly improved when the mass is taken as a free parameter, and for the models with a Kerr BH good fits were obtained for most sources of the present sample. In Figure 1, we compare the BH masses obtained by the accretion-disk model and by reverberation-mapping. We find that for one third of the objects, the reverberation-based BH mass is clearly below the accretion-disk BH mass while in other two thirds, the two agree. Furthermore, it was found that for those objects where the reverberation-based mass deviated from the AD model mass, using the reverberation-based mass combined with a high accretion rate (i.e. 0.3) still falls far below the total energy budget. So, we conclude that, in view of the energy budget the BH mass based on reverberation-mapping may be underestimated. Due to lack of knowledge of the detailed structure and dynamics of the BLR, the BH mass based on reverberation-mapping would suffer from the assumption of the constant scale factor f. Possible systematic uncertainties in the reverberation-mapping measurements have been intensively discussed. Krolik (2001) pointed out that orientation effects (assuming a disk-like BLR) would lead to an underestimation of the BH mass by at least one order of magnitude for objects with low inclination, but the orientation effects,

Table 2 Fitting Results with BH Masses from Reverberation-mapping

		Schwarzschild Black Hole			Kerr Black Hole			
Name	$\log m_\bullet$	$\dot{m}$	$\cos\Theta$	χ^2/d.o.f.	$\dot{m}$	$\cos\Theta$	χ^2/d.o.f.	β_1
PG 0003+199	$7.15^{+0.10}_{-0.13}$	$0.30^{-}_{-0.16}$	$0.99^{-}_{-0.20}$	6907./12	$0.22^{-}_{-0.15}$	0.70 ± 0.23	8058./12	0.9
PG 0026+129	$8.59^{+0.09}_{-0.12}$	0.16 ± 0.06	$0.93^{-}_{-0.15}$	26.6/32	0.20 ± 0.05	$0.99^{-}_{-0.16}$	105./32	1.4
PG 0052+251	$8.57^{+0.08}_{-0.10}$	0.22 ± 0.06	$0.92^{-}_{-0.12}$	29.8/34	$0.24^{-}_{-0.08}$	$0.99^{-}_{-0.15}$	158./34	1.4
PG 0804+761	$8.84^{+0.05}_{-0.06}$	0.10 ± 0.04	$0.90^{-}_{-0.16}$	69.1/32	$0.21^{-}_{-0.06}$	$0.92^{-}_{-0.14}$	54.5/32	1.4
PG 0844+349	$7.97^{+0.15}_{-0.23}$	$0.20^{-}_{-0.10}$	$0.99^{-}_{-0.30}$	131./34	$0.20^{-}_{-0.12}$	$0.99^{-}_{-0.32}$	341./3	1.2
PG 0953+414	$8.44^{+0.08}_{-0.10}$	$0.30^{-}_{-0.15}$	$0.92^{-}_{-0.25}$	311./31	$0.22^{-}_{-0.12}$	0.75 ± 0.20	455./31	1.4
PG 1211+143	$8.16^{+0.11}_{-0.16}$	$0.30^{-}_{-0.15}$	$0.99^{-}_{-0.32}$	1404./35	$0.20^{-}_{-0.11}$	$0.99^{-}_{-0.35}$	2491./35	1.1
PG 1226+023	$8.95^{+0.08}_{-0.10}$	$0.30^{-}_{-0.12}$	$0.99^{-}_{-0.15}$	219./10	$0.25^{-}_{-0.10}$	$0.90^{-}_{-0.15}$	400./10	1.0
PG 1229+204	$7.86^{+0.17}_{-0.28}$	$0.30^{-}_{-0.09}$	$0.76^{-}_{-0.15}$	213./33	0.19 ± 0.08	$0.99^{-}_{-0.20}$	355./33	1.4
PG 1307+085	$8.64^{+0.11}_{-0.14}$	$0.25^{-}_{-0.08}$	0.70 ± 0.20	30.7/36	$0.25^{-}_{-0.09}$	$0.99^{-}_{-0.22}$	45.6/36	1.2
PG 1411+442	$8.65^{+0.12}_{-0.17}$	$0.06^{+0.04}_{-}$	$0.80^{-}_{-0.20}$	42.3/34	0.18 ± 0.07	$0.99^{-}_{-0.22}$	50.6/34	1.2
PG 1426+015	$9.11^{+0.11}_{-0.15}$	$0.04^{+0.05}_{-}$	0.30 ± 0.15	75.9/37	$0.08^{+0.06}_{-}$	0.30 ± 0.20	117./37	1.4
PG 1613+658	$8.45^{+0.17}_{-0.27}$	$0.30^{-}_{-0.12}$	$0.99^{-}_{-0.30}$	416./89	$0.28^{-}_{-0.15}$	$0.99^{-}_{-0.35}$	1804./89	1.2
PG 1617+175	$8.77^{+0.09}_{-0.11}$	$0.03^{+0.05}_{-}$	0.65 ± 0.15	62.0/46	0.11 ± 0.07	0.75 ± 0.20	96.5/46	1.4
PG 1700+518	$8.89^{+0.09}_{-0.10}$	$0.30^{-}_{-0.10}$	$0.99^{-}_{-0.25}$	211./36	$0.27^{-}_{-0.08}$	$0.99^{-}_{-0.20}$	100./36	1.4
PG 2130+099	$8.66^{+0.05}_{-0.06}$	$0.04^{+0.04}_{-}$	0.70 ± 0.20	82.1/35	0.10 ± 0.04	$0.99^{-}_{-0.20}$	32.1/35	1.2
Mrk 79	$7.72^{+0.11}_{-0.14}$	$0.05^{+0.04}_{-}$	$0.80^{-}_{-0.20}$	44.2/8	0.19 ± 0.06	$0.99^{-}_{-0.25}$	60.4/8	1.3
Mrk 110	$7.40^{+0.09}_{-0.12}$	$0.27^{-}_{-0.12}$	$0.85^{-}_{-0.25}$	132./4	$0.23^{-}_{-0.10}$	$0.98^{-}_{-0.22}$	86.7/4	1.3
Mrk 279	$7.54^{+0.10}_{-0.13}$	$0.25^{-}_{-0.10}$	$0.92^{-}_{-0.30}$	536./20	0.10 ± 0.06	$0.97^{-}_{-0.35}$	1409./20	1.2
Mrk 509	$8.16^{+0.03}_{-0.04}$	0.20 ± 0.05	0.50 ± 0.15	2.7/11	0.19 ± 0.07	$0.99^{-}_{-0.22}$	0.85/11	1.2
Mrk 590	$7.68^{+0.06}_{-0.07}$	$0.20^{-}_{-0.10}$	$0.92^{-}_{-0.20}$	138./7	0.15 ± 0.11	$0.99^{-}_{-0.30}$	449./7	1.2
Mrk 817	$7.69^{+0.06}_{-0.07}$	$0.20^{-}_{-0.12}$	$0.94^{-}_{-0.20}$	304./6	0.10 ± 0.07	$0.93^{-}_{-0.25}$	392./6	1.4
NGC 3227	$7.63^{+0.18}_{-0.31}$	0.16 ± 0.10	$0.80^{-}_{-0.30}$	285./5	0.12 ± 0.08	$0.92^{-}_{-0.30}$	120./5	1.2
NGC 3516	$7.63^{+0.13}_{-0.18}$	$0.20^{-}_{-0.13}$	$0.76^{-}_{-0.25}$	9176./27	0.12 ± 0.08	$0.99^{-}_{-0.20}$	218./27	1.1
NGC 3783	$7.47^{+0.07}_{-0.09}$	$0.08^{+0.05}_{-}$	0.70 ± 0.15	12.2/11	0.19 ± 0.06	$0.99^{-}_{-0.18}$	13.8/9	1.0
NGC 4051	$6.28^{+0.15}_{-0.23}$	0.15 ± 0.06	$0.92^{-}_{-0.22}$	22.3/13	$0.25^{-}_{-0.05}$	$0.99^{-}_{-0.18}$	11.3/13	1.4
NGC 4151	$7.12^{+0.13}_{-0.18}$	0.17 ± 0.06	$0.85^{-}_{-0.18}$	18.1/12	0.20 ± 0.05	$0.99^{-}_{-0.20}$	14.5/7	1.1
NGC 4593	$6.99^{+0.09}_{-0.10}$	$0.24^{-}_{-0.10}$	0.40 ± 0.20	162./5	0.15 ± 0.10	$0.99^{-}_{-0.25}$	405./5	1.2
NGC 5548	$7.83^{+0.02}_{-0.02}$	$0.22^{-}_{-0.13}$	0.64 ± 0.25	1193./16	0.19 ± 0.10	$0.98^{-}_{-0.25}$	253./16	1.3
NGC 7469	$7.09^{+0.05}_{-0.05}$	0.12 ± 0.10	0.40 ± 0.25	2549./15	$0.19^{-}_{-0.12}$	$0.92^{-}_{-0.30}$	2509./15	1.2
3C 120	$7.74^{+0.19}_{-0.23}$	$0.24^{-}_{-0.08}$	0.76 ± 0.20	47.0/7	0.19 ± 0.09	$0.99^{-}_{-0.22}$	166./7	1.0
3C390.3	$8.46^{+0.09}_{-0.11}$	0.13 ± 0.08	$0.16^{+0.26}_{-}$	58.9/41	0.12 ± 0.06	0.50 ± 0.20	23.7/41	1.2
Akn 120	$8.18^{+0.05}_{-0.06}$	0.20 ± 0.05	0.40 ± 0.15	5.1/5	$0.25^{-}_{-0.05}$	$0.99^{-}_{-0.20}$	5.6/5	1.2
IC 4329A	$7.00^{+0.45}_{-}$	$0.27^{-}_{-0.09}$	$0.80^{-}_{-0.25}$	20.5/4	$0.27^{-}_{-0.10}$	$0.99^{-}_{-0.30}$	52.0/4	1.0
Fairall 9	$8.41^{+0.09}_{-0.11}$	0.19 ± 0.09	$0.70^{-}_{-0.30}$	207./18	$0.20^{-}_{-0.10}$	$0.80^{-}_{-0.35}$	280./18	1.8

NOTES/REFERENCES:– (1) source name; (2) BH mass estimated from reverberation mapping (Peterson et al. 2004), (the BH mass of NGC4593 from Denney et al. (2006)). For the PG quasars, the given values of χ^2/d.o.f. excluding data from Kaspi et al. (2000), but residuals from these data displayed in Fig. 1; (3)–(5) fits by Sch. BH disk models; (6)–(8) fits by Kerr BH disk models; (9) the index of IR power law, and a uniform uncertainty of ± 0.1 is adopted.

argued by Collin et al. (2006), play a role only in some subsets of AGNs. They suggested that the Eddington ratio may be the dominant parameter in determining the properties of BLR, and may be responsible for the discrepancies between the two mass estimations.

III) The factor f is defined as the ratio of the BH mass from the accretion disk to that from the reverberation mapping,

$$f = \frac{M_\bullet(\mathrm{AD})}{M_\bullet(\mathrm{RM})} \langle f \rangle \,. \tag{6}$$

Onken et al. (2004) obtained an average value, $\langle f \rangle = 5.5/4$, and Peterson et al. (2004) applied it to an AGN sample. Figure 2 (left panel) plots f against the Eddington ratios ($L_{\rm bol}/L_{\rm Edd}$), obtained in the reverberation mapping technique. We find that, for two thirds of the sample with for $L_{\rm Bol}/L_{\rm Edd} < 0.1$, $f/\langle f \rangle \approx 1$,

Table 3 Fitting Results Based on AD Models

	Schwarzschild Black Hole				Kerr Black Hole				
Name	$\log m_\bullet$	$\dot{m}$	$\cos\Theta$	χ^2/d.o.f.	$\log m_\bullet$	$\dot{m}$	$\cos\Theta$	χ^2/d.o.f.	$f/\langle f\rangle$
PG 0003+199*	$8.05^{+0.08}_{-0.10}$	0.10 ± 0.04	$0.90^{-}_{-0.12}$	56.4/11	$8.48^{+0.07}_{-0.09}$	0.10 ± 0.02	0.75 ± 0.10	14.3/11	9.08 ± 2.98
PG 0026+129	$8.78^{+0.09}_{-0.11}$	0.12 ± 0.03	0.80 ± 0.10	4.6/31	$8.96^{+0.07}_{-0.09}$	0.14 ± 0.04	0.80 ± 0.10	4.7/31	2.34 ± 0.71
PG 0052+251	$8.78^{+0.10}_{-0.12}$	0.12 ± 0.03	$0.92^{-}_{-0.10}$	8.9/33	$9.08^{+0.07}_{-0.09}$	0.18 ± 0.04	$0.92^{-}_{-0.10}$	7.2/33	3.25 ± 0.89
PG 0804+761	$8.80^{+0.07}_{-0.08}$	0.10 ± 0.03	$0.99^{-}_{-0.10}$	65.8/31	$8.85^{+0.06}_{-0.07}$	0.20 ± 0.05	$0.92^{-}_{-0.10}$	55.5/31	1.02 ± 0.20
PG 0844+349	$8.30^{+0.16}_{-0.26}$	$0.08^{+0.06}_{-}$	$0.90^{-}_{-0.25}$	33.9/33	$8.70^{+0.13}_{-0.19}$	0.10 ± 0.06	0.75 ± 0.20	37.8/33	5.42 ± 2.93
PG 0953+414	$9.00^{+0.12}_{-0.16}$	0.20 ± 0.07	0.75 ± 0.20	16.5/30	$9.08^{+0.10}_{-0.13}$	$0.24^{-}_{-0.09}$	0.75 ± 0.20	33.2/30	4.35 ± 1.46
PG 1211+143	$8.77^{+0.10}_{-0.13}$	0.10 ± 0.03	$0.99^{-}_{-0.22}$	43.6/34	$8.83^{+0.08}_{-0.10}$	0.15 ± 0.04	$0.80^{-}_{-0.20}$	43.6/34	4.66 ± 1.68
PG 1226+023	$9.48^{+0.08}_{-0.10}$	0.12 ± 0.03	0.84 ± 0.15	11.9/9	$9.48^{+0.07}_{-0.09}$	0.22 ± 0.04	$0.99^{-}_{-0.16}$	11.1/9	3.40 ± 0.94
PG 1229+204	$8.30^{+0.13}_{-0.18}$	0.10 ± 0.04	$0.92^{-}_{-0.22}$	56.6/32	$8.49^{+0.08}_{-0.10}$	0.18 ± 0.06	$0.99^{-}_{-0.20}$	37.5/32	4.25 ± 2.21
PG 1307+085	$8.73^{+0.11}_{-0.15}$	0.10 ± 0.06	$0.99^{-}_{-0.30}$	7.2/35	$8.73^{+0.11}_{-0.15}$	$0.30^{-}_{-0.15}$	$0.99^{-}_{-0.30}$	64.1/35	1.23 ± 0.50
PG 1411+442	$8.48^{+0.13}_{-0.19}$	$0.06^{+0.05}_{-}$	$0.75^{-}_{-0.25}$	90.2/33	$8.70^{+0.11}_{-0.15}$	0.15 ± 0.07	$0.99^{-}_{-0.22}$	44.1/33	1.13 ± 0.50
PG 1426+015	$9.08^{+0.11}_{-0.14}$	$0.04^{+0.06}_{-}$	0.30 ± 0.15	108./36	$9.23^{+0.08}_{-0.10}$	$0.08^{+0.05}_{-}$	0.30 ± 0.10	29.9/36	1.31 ± 0.47
PG 1613+658	$8.78^{+0.12}_{-0.17}$	$0.08^{+0.06}_{-}$	$0.90^{-}_{-0.30}$	139./88	$8.99^{+0.08}_{-0.10}$	0.16 ± 0.06	$0.99^{-}_{-0.30}$	138./88	3.55 ± 1.79
PG 1617+175	$8.60^{+0.10}_{-0.14}$	$0.04^{+0.06}_{-}$	$0.80^{-}_{-0.20}$	75.5/45	$8.80^{+0.07}_{-0.09}$	0.10 ± 0.04	$0.80^{-}_{-0.20}$	61.9/45	1.06 ± 0.31
PG 1700+518	$9.00^{+0.12}_{-0.17}$	$0.30^{-}_{-0.11}$	$0.99^{-}_{-0.22}$	62.4/35	$9.40^{+0.08}_{-0.10}$	0.20 ± 0.06	0.80 ± 0.16	30.1/35	$3.21^{+0.99}_{-0.93}$
PG 2130+099	$8.60^{+0.05}_{-0.06}$	$0.05^{+0.04}_{-}$	0.75 ± 0.20	130./35	$8.74^{+0.04}_{-0.05}$	0.10 ± 0.03	0.80 ± 0.15	32./35	1.20 ± 0.19
Mrk 79	$7.63^{+0.12}_{-0.16}$	0.10 ± 0.05	$0.75^{-}_{-0.25}$	60.5/7	$7.78^{+0.08}_{-0.10}$	0.17 ± 0.06	$0.99^{-}_{-0.23}$	43.3/7	1.15 ± 0.39
Mrk 110	$7.48^{+0.08}_{-0.10}$	$0.20^{-}_{-0.12}$	$0.99^{-}_{-0.35}$	221./3	$7.44^{+0.08}_{-0.10}$	0.18 ± 0.10	$0.99^{-}_{-0.30}$	78.0/3	1.10 ± 0.35
Mrk 279	$8.00^{+0.13}_{-0.19}$	0.10 ± 0.05	$0.99^{-}_{-0.30}$	41.2/19	$8.30^{+0.08}_{-0.10}$	0.10 ± 0.04	$0.99^{-}_{-0.20}$	22.9/19	5.76 ± 1.91
Mrk 509	$8.15^{+0.10}_{-0.14}$	$0.05^{+0.04}_{-}$	$0.90^{-}_{-0.20}$	7.5/10	$8.28^{+0.08}_{-0.10}$	0.10 ± 0.04	$0.99^{-}_{-0.20}$	3.3/10	1.33 ± 0.29
Mrk 590	$7.78^{+0.08}_{-0.10}$	$0.25^{-}_{-0.09}$	$0.99^{-}_{-0.30}$	200./6	$7.75^{+0.08}_{-0.10}$	0.18 ± 0.07	$0.99^{-}_{-0.30}$	170./6	1.19 ± 0.30
Mrk 817*	$8.60^{+0.08}_{-0.10}$	$0.08^{+0.06}_{-}$	0.74 ± 0.15	254./4	$8.70^{+0.08}_{-0.10}$	0.10 ± 0.07	0.50 ± 0.20	171./4	1.00 ± 0.22
NGC 3227	$7.71^{+0.11}_{-0.14}$	$0.05^{+0.04}_{-}$	$0.80^{-}_{-0.30}$	113./4	$7.69^{+0.10}_{-0.12}$	0.10 ± 0.06	$0.99^{-}_{-0.25}$	94.8/4	1.15 ± 0.65
NGC 3516	$7.64^{+0.11}_{-0.15}$	0.12 ± 0.10	$0.70^{-}_{-0.30}$	3095./26	$7.70^{+0.10}_{-0.12}$	0.12 ± 0.08	$0.99^{-}_{-0.30}$	78.3/26	1.16 ± 0.49
NGC 3783*	$8.00^{+0.08}_{-0.10}$	0.20 ± 0.05	0.55 ± 0.20	5.7/4	$8.00^{+0.08}_{-0.10}$	0.10 ± 0.04	$0.99^{-}_{-0.25}$	9.9/10	1.00 ± 0.26
NGC 4051	$6.30^{+0.11}_{-0.14}$	$0.25^{-}_{-0.10}$	$0.75^{-}_{-0.30}$	25.7/12	$6.34^{+0.10}_{-0.12}$	0.20 ± 0.07	$0.99^{-}_{-0.25}$	18.8/12	1.15 ± 0.55
NGC 4151*	$7.72^{+0.09}_{-0.12}$	$0.05^{+0.04}_{-}$	$0.85^{-}_{-0.25}$	9.5/14	$7.90^{+0.08}_{-0.10}$	0.10 ± 0.05	$0.85^{-}_{-0.20}$	15.7/13	1.00 ± 0.49
NGC 4593*	$8.00^{+0.09}_{-0.12}$	$0.20^{-}_{-0.10}$	$0.92^{-}_{-0.20}$	2.2/2	$7.60^{+0.08}_{-0.10}$	0.10 ± 0.06	$0.99^{-}_{-0.25}$	24.8/2	$1.00^{+0.33}_{-0.29}$
NGC 5548	$7.89^{+0.08}_{-0.10}$	0.10 ± 0.07	$0.80^{-}_{-0.28}$	922./15	$7.89^{+0.08}_{-0.10}$	0.16 ± 0.10	$0.99^{-}_{-0.27}$	444./15	1.16 ± 0.24
NGC 7469	$8.00^{+0.06}_{-0.07}$	0.10 ± 0.04	0.50 ± 0.20	11.0/9	$7.95^{+0.06}_{-0.07}$	0.17 ± 0.06	$0.99^{-}_{-0.22}$	14.7/10	7.39 ± 1.39
3C 120	$7.81^{+0.11}_{-0.15}$	$0.20^{-}_{-0.10}$	$0.80^{-}_{-0.25}$	104./6	$7.81^{+0.11}_{-0.14}$	$0.23^{-}_{-0.09}$	$0.99^{-}_{-0.25}$	91.8/6	$1.17^{+0.74}_{-0.58}$
3C390.3	$8.47^{+0.11}_{-0.14}$	0.10 ± 0.07	$0.80^{-}_{-0.30}$	238./40	$8.30^{+0.11}_{-0.14}$	0.15 ± 0.04	0.70 ± 0.22	23.9/40	0.70 ± 0.25
Akn 120	$8.08^{+0.12}_{-0.17}$	0.10 ± 0.04	0.75 ± 0.23	7.1/4	$8.29^{+0.08}_{-0.10}$	0.17 ± 0.05	$0.99^{-}_{-0.20}$	2.2/4	1.31 ± 0.31
IC 4329A*	$8.00^{+0.08}_{-0.10}$	$0.28^{-}_{-0.15}$	$0.80^{-}_{-0.30}$	6.1/6	$8.00^{+0.08}_{-0.10}$	$0.23^{-}_{-0.10}$	$0.99^{-}_{-0.30}$	3.6/2	$1.00^{+1.83}_{-}$
Fairall 9	$8.51^{+0.08}_{-0.10}$	$0.08^{+0.05}_{-}$	$0.75^{-}_{-0.25}$	93.2/17	$8.48^{+0.08}_{-0.10}$	0.20 ± 0.07	$0.80^{-}_{-0.25}$	98.5/17	1.18 ± 0.35

NOTES/REFERENCES:–

Ref: The values of $f/\langle f\rangle$ are calculated by using the corresponding Kerr BH masses. For sources marked with '*', due to large variabilities in their luminosities, we consider their reverberation mapping based masses as the reliable BH masses, and then give their $f/\langle f\rangle$ values equal 1.0. With the exception of PG0003, we refit its emergent spectrum using the luminosity of 5100Å given by Peterson et al. (2004) to obtain a Kerr BH mass of $8.11^{+0.08}_{-0.10}$ as the BH mass for calculating its $f/\langle f\rangle$.

while for $L_{\rm Bol}/L_{\rm Edd} > 0.1$, we have (1) f deviates significantly from ≈ 1, and increases with increasing Eddington ratio (though with large scatters), and (2) there is a very strong correlation between f and $L_{\ 5100}$ (see the right panel):

$$f/\langle f\rangle = 6.0 L_{44}^{-1/5}, \tag{7}$$

where $L_{44} = L_{5100}/10^{44}{\rm erg\ s^{-1}}$, with a Pearson coefficient $r = 0.7$. We also find that most of the objects with $f/\langle f\rangle > 1$ tend to have narrower FWHM (Hβ) (i.e. $\lesssim 4000\ {\rm km\ s^{-1}}$) and higher Eddington ratio than those with lower $f/\langle f\rangle$ values. Almost none of the objects with $f/\langle f\rangle \approx 1$ has FWHM (Hβ) less than $2000\ {\rm km\ s^{-1}}$, and some have FWHM (Hβ) more than $4000\ {\rm km\ s^{-1}}$. The relation between f and FWHM (Hβ) is further displayed in Figure 3, where we include all objects with $\chi^2_\nu \leq 1.5$ in the accretion disk model containing a Kerr BH.

We now check the uncertainties in the spectral fits. In the fitting procedures, the intrinsic extinction of the sources is set to zero. To examine the uncertainty caused by intrinsic reddening, we assume the reddening value of $E(B-V) \sim 0.05$, which leads to an increase in the accretion rate by approximately

Table 4 Models and Fits for X-ray Bands

Name (1)	$N_{\rm H}^{\rm in}$ (2)	kT (3)	Γ_1 (4)	Γ_2 (5)	E_k (6)	$E_{\rm edge}$ (7)	τ (8)	$EW_{K\alpha}$ (9)	${\chi^2}_\nu$/d.o.f. (10)
PG 0003+199^A	–	122 ± 1	2.25 ± 0.01	–	–	0.64 ± 0.02	0.17 ± 0.01	–	1.20/967
PG 0052+251^B	–	–	2.49 ± 0.04	1.80 ± 0.02	1.75 ± 0.06	–	–	–	0.99/625
PG 0844+349^A	–	113 ± 1	2.19 ± 0.01	–	–	–	–	–	1.07/493
PG 0953+414^B	–	–	2.66 ± 0.05	2.07 ± 0.02	1.50 ± 0.01	–	–	–	1.05/411
PG 1211+143^C	–	110 ± 1	1.60 ± 0.02	240 ± 2	-	0.77 ± 0.02	0.49 ± 0.02	–	1.10/748
PG 1226+023^B	–	–	2.14 ± 0.02	1.74 ± 0.01	1.39 ± 0.02	–	–	–	1.08/1501
PG 1229+204^B	–	–	2.57 ± 0.04	1.92 ± 0.02	1.75 ± 0.07	–	–	–	1.07/487
PG 1307+085^A	6.17 ± 0.03	105 ± 1	1.53 ± 0.03	–	–	0.74 ± 0.01	0.53 ± 0.13	–	1.01/223
PG 1411+442^D	$58.33 \pm 0.14^*$	125 ± 7	1.62 ± 0.25	–	–	–	–	0.18 ± 0.09	0.84/103
PG 1426+015^B	0.26 ± 0.13	–	2.59 ± 0.10	1.96 ± 0.04	1.56 ± 0.01	–	–	–	1.07/203
PG 1613+658^B	11.72 ± 0.05	–	2.79 ± 0.55	2.57 ± 0.61	1.40 ± 0.11	–	–	–	0.45/98
PG 2130+099^A	0.18 ± 0.01	112 ± 1	1.64 ± 0.01	–	–	0.74 ± 0.01	0.22 ± 0.03	–	1.26/547
Mrk 79^D	$26.30 \pm 0.05^*$	111 ± 5	1.73 ± 0.04	–	–	–	–	–	1.08/442
Mrk 110^D	$4.68 \pm 0.01^*$	120 ± 1	1.99 ± 0.01	–	–	–	–	–	1.19/870
Mrk 509^D	$9.11 \pm 0.01^*$	110 ± 1	1.94 ± 0.01	–	–	–	–	0.11 ± 0.01	1.29/1557
Mrk 590^B	0.49 ± 0.01	–	2.41 ± 0.11	1.64 ± 0.03	1.56 ± 0.07	–	–	–	0.99/338
NGC 3227^A	22.51 ± 0.04	803 ± 206	1.72 ± 0.06	2.21 ± 0.17	–	–	–	-	0.98/166
NGC 3516^D	$25.90 \pm 0.01^*$	124 ± 2	1.41 ± 0.01	–	–	–	–	0.09 ± 0.01	1.31/1770
NGC 3783^D	$47.97 \pm 0.01^*$	114 ± 21	1.65 ± 0.01	–	–	–	–	0.06 ± 0.01	3.20/2073
NGC 4051^E	$32.72 \pm 0.02^*$	144 ± 1	2.67 ± 0.06	1.49 ± 0.01	1.56 ± 0.01	0.58 ± 0.02	0.25 ± 0.03	-	1.40/926
NGC 4151^F	$52.19 \pm 0.01^*$	127 ± 1	0.88 ± 0.02	23 ± 1	–	7.22 ± 0.02	0.28 ± 0.01	-	1.65/1960
NGC 4593^A	8.66 ± 0.09	98 ± 9	1.78 ± 0.17	–	–	–	–	–	0.58/40
NGC 5548^D	$11.31 \pm 0.01^*$	106 ± 1	1.71 ± 0.01	–	–	–	–	–	1.18/1252
NGC 7469^D	$277.5 \pm 0.22^*$	110 ± 3	1.93 ± 0.01	–	–	–	–	0.08 ± 0.01	1.40/1680
$3C120^D$	$6.74 \pm 0.03^*$	154 ± 3	1.77 ± 0.02	–	–	-	–	–	1.30/1038
$3C390.3^D$	$12.13 \pm 0.01^*$	156 ± 2	1.74 ± 0.01	–	–	–	–	–	1.19/1655
Akn 120^D	$15.49 \pm 0.17^*$	110 ± 4	2.18 ± 0.01	–	–	–	–	0.11 ± 0.03	1.50/1862
Fairall 9^A	–	117 ± 2	1.83 ± 0.01	–	–	–	–	–	1.12/1012

NOTES/REFERENCES:– (1) source name; (2) intrinsic absorption (ionized absorption component marked with '*') $N_{\rm H}^{\rm in}$ values in $10^{20}\ cm^{-2}$; (3) temperature of black body in eV; (4) power law spectral index; (5) power law spectral index; (6) break energy for broken power law model in keV; (7) absorption edge energy in keV; (8) absorption edge depth; (9) $EW_{K\alpha}$ (in keV) of $F_eK\alpha$ line fixed at 6.4 keV; (10) ${\chi^2}_\nu$/d.o.f. values.
Ref: A: black body plus power law model; B: broken power law model; C: double black body plus power law model; D: model A with ionized absorption component (ABSORI in XSPEC); E: black body plus broken power law model with ionized absorption component (ABSORI in XSPEC); F: model C with ionized absorption component (ABSORI in XSPEC).

15% and an increase in the mass less than 5%. In addition, for low luminosity sources (7/35), the flux contribution from host galaxy would be more than 30 per cent in the near IR/optical bands (Bentz et al. 2006), and correction for this effect would lead to an uncertainty of the mass around 30 per cent. On the other hand, comptonization could affect the far UV spectral shape. The recent composite *HST/FUSE* spectra of low redshift PG quasars display a turn-down at far-UV (Zheng et al. 1997; Shang et al. 2005), and such spectral feature has also been revealed by a very large sample from GALEX (Trammell et al. 2007). The accretion disk spectrum is expected to reprocess the AGN SED from the optical to the soft X-ray range, with the maximum emission in the far UV. The dependence of the spectral shape on the model parameters is such that, a high accretion rate and viscosity could make the spectrum harder, while changing from face-on to edge-on orientation of the disk could reduce the total flux from the disk and harden the spectrum due to the Doppler boosting effect, and it has been found from grid calculations that emissions in different energy bands actually come from different radii. The optical/UV emission spectrum originated from regions in the relatively outer part of the disk, whereas the far UV emission deviates significantly from the spectra expected in the disk models and is more sensitive to the accretion rate, indicating that the structure of the inner disk is extremely complicated. In addition, the FUV/soft X-ray emissions would be complicated by emissions from different ion abundances, which is not considered in the accretion disk that assumed a pure hydrogen atmosphere. So, the BH masses are deduced from fitting the optical/UV spectra and are thought to be reliable. We plan to consider theoretical models that focus on the structure of the inner disk in our future work.

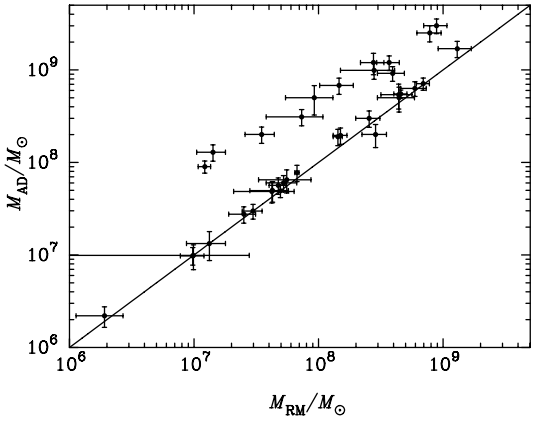

Fig. 1 Masses estimated based on accretion disk models ($M_{\rm AD}$) around Kerr BHs plotted versus masses based on reverberation-mapping ($M_{\rm RM}$) for all objects in Table 1. The straight line traces the diagonals.

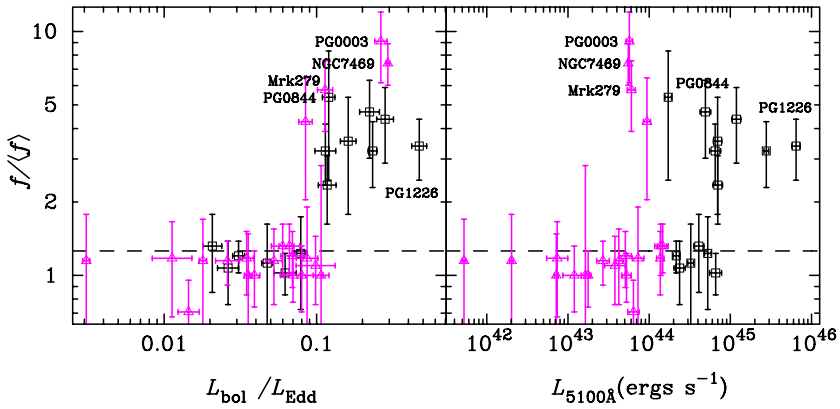

Fig. 2 Factor f plotted against the Eddington ratios and optical luminosities. The red triangles indicate the objects with $\log\lambda L_{5100} \leqslant 44.2$, i.e. Seyfert nuclei, and the black squares PG quasars. There are two features in the plot: 1) A significant deviation from the standard value $\langle f\rangle$ when the Eddington ratio is larger than 0.1 and a weak correlation appears; 2) A strong correlation between f and $L_{5100\text{Å}}$. Luminosities in 5100Å are taken from Peterson et al. (2004).

4 DISCUSSION

4.1 Disk Wind in BLR

The factor f shows us about the geometry of the BLR. It takes a value of 0.75 if the BLR is isotropic (Kaspi et al. 2000; Peterson et al. 2004; Kaspi et al. 2005). With the calibration by the $M_\bullet - \sigma$ relation (Tremaine et al. 2002), it was found that the average for 16 Seyfert galaxies is $\langle f\rangle = 5.5/4$ (Onken et al. 2004), with however, some rather large scatter. A similar value of $\langle f\rangle = 1.12$ was given by the X-ray excess variance method (Nikolajuk et al. 2006). We also found that the objects with $L_{\rm Bol}/L_{\rm Edd} < 0.1$ have a mean value of fe, approximately equal to that obtained by Onken et al. (2004). All these results indicate that the BRL is rather flat since in all cases which values of f are larger than 0.75, corresponding to a spherical geometry. On the other hand, with the increased $L_{\rm Bol}/L_{\rm Edd}$ (> 0.1), the factor f diverges from $\langle f\rangle$. It strongly implies that the BLRs in AGNs may vary across individual sources and strongly depend on the Eddington ratio, with

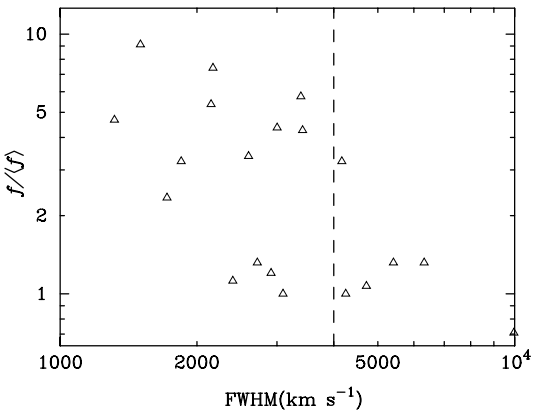

Fig. 3 Factor f versus FWHM (Hβ) in the rms spectrum from Collin et al. (2006), for objects with Kerr BH masses fitted well by the AD models ($\chi^2_\nu \leq 1.5$). Objects with $f/\langle f\rangle > 1$ tend to have FWHM (Hβ) $\lesssim 4000\ \mathrm{km\ s^{-1}}$. The dashed vertical line marks FWHM (Hβ)$= 4000\ \mathrm{km\ s^{-1}}$.

clearly different geometric factors between objects of high and low Eddington ratios, roughly on either side of the value ~ 0.1. The dependence of BLR geometry on the Eddington ratio is briefly examined as follows.

For a BLR with a flattened disk, the factor f reads (Collin et al. 2006; Wu & Han 2001),

$$f = \left[\sin^2 i + (H/R)^2\right]^{-1}, \tag{8}$$

where i is the inclination angle to the observer, H the height of the disk at radius R. When $H/R \approx 1$ dominates over $\sin i$, $f \approx 1$, the BLR shows a quasi-spherical geometry whatever the inclination. However, $f \approx (R/H)^2$ for the case of $H/R < 1$ when the BLR is close to being face-on. For a flattened-disk-dominated BLR, the outer region of the disk is ruled out since its thickness is too small (typically thinner than $H/R < 10^{-3}$) to have large enough covering factor (typically 0.1) (Shakura et al. 1973). The self-gravity-dominated disk can be also ruled out since it is thinner than the Shakura-Sunyaev disk (Goodman et al. 2003). So, the BLR is unlikely to be a very thin flat structure which is entirely dominated by the Keplerian rotation, as suggested by Collin et al. (2006).

Actually, when the Eddington ratio is high enough, disk winds will inevitably occur, and their presence is fully supported by evidence from the properties of CIVλ 1549 emission line (Vestergaard et al. 2000). The disk wind has been suggested to model the BLR (Murray et al. 1995), which is parallel to the disk surface so increasing the thickness of the disk, Hence the thickness should be a function of the luminosity. According to the wind theory (Murray et al. 1995), the scale of the wind as the BLR is $H/R \sim 0.1 L_{46}^{1/2} M_8^{-1} r_4^{-1}$, where $L_{46} = L/10^{46}\mathrm{erg\ s^{-1}}$, $M_8 = M_\bullet/10^8 M_\odot$, $r_4 = R/10^4 R_g$ and $R_g = 2GM_\bullet/c^2$. This relation gives a very sensitive relation $f \propto L_{46}^{-1}$. Though it is steeper than the relation given by Figure 3, the trend clearly supports the disk wind scenario when the Eddington ratio is high enough. If the BLR is developed from disk winds, then we can assume the wind velocity to be

$$v_{\rm win} = k_0 \dot{m}^\gamma v_{\rm Kep}, \tag{9}$$

where k_0 is a constant and γ also a constant. This phenomenological formula assumes that the wind velocity increases with increasing Eddington ratio. For a viewing angle i, the observed FWHM is $v_{\rm obs} \sim v_{\rm win} \cos i$, and we finally have ($\gamma > 0$)

$$M_\bullet = k_0 \dot{m}^\gamma \cos^2 i \frac{(c\Delta\tau) v_{\rm Kep}^2}{G}, \tag{10}$$

and

$$f = k_0 \dot{m}^\gamma \cos^2 i = (k_0/2)\dot{m}^\gamma, \tag{11}$$

where $\langle \cos^2 i \rangle = 1/2$. This relation can explain well the dependence of f on the Eddington ratios. Based on a 2D simulation of the BLR (Huré 1998; Collin et al. 2006), the BLR structure was found to be correlated with the Eddington ratio: when $L_{\rm Bol}/L_{\rm Edd} > 0.1$, the BLR becomes gravitationally unstable, and wind may then be launched. However, both the formation of disk wind and its dependence on the physical parameters such as the Eddington ratio, bolometric luminosity, etc., are very likely to be more complicated, and require more sophisticated modelling.

4.2 Influence of Eddington Ratio on the BLR

Two AGN populations, i.e., Population A with FWHM (Hβ) $\lesssim 4000$ km s^{-1}, and Population B with FWHM (Hβ) $\gtrsim 4000$ km s^{-1}, have been intensively investigated (Sulentic et al. 2000a; Marziani et al. 2003; see also Collin et al. 2006). Interestingly, the distributions of Eddington ratios in the two populations are distinctly different: Pop. A objects tend to have higher Eddington ratios, and Pop. B objects, lower Eddington ratios, about a value ~ 0.15 (Marziani et al. 2003). It is speculated that the different properties in Pop. A and Pop. B may stem from structural differences in the BLR (Sulentic et al. 2000b; Marziani et al. 2006): for Pop. A objects, the geometry of the BLR has the disk and wind configuration, while for Pop. B, the wind scenario would be less supported in a generally unclear BLR structure. We confirm the findings presented by Sulentic et al. in two aspects: 1) The presence of two kinds of BLR geometry, and 2) Its dependence on the Eddington ratio, with a critical value of $L_{\rm Bol}/L_{\rm Edd} \sim 0.1$. The wind properties are also expected to be connected with the Eddington ratio. Based on the present results, we suggest that high Eddington ratios would enable the triggering of strong winds in the BLR, so stronger winds go with higher Eddington ratios (see Fig. 2). Taking into account the gravitational instability intrinsic to the disk structure, we briefly discuss a plausible interpretation which has been speculated by many authors (e.g., Collin et al. 2006). Consider the state of the disk in the outer regions. When the self-gravity of disk becomes greater than the vertical component of the central gravity, the disk can be broken into self-gravitating clumps, and these clumps can contribute to the formation of disk wind. It is suggested that when $L_{\rm Bol}/L_{\rm Edd} > 0.1$ (Huré 1998; Collin et al. 2006), the BLR tends to be gravitationally unstable, and the influence of wind will be more considerable. On the other hand, for objects with low Eddington ratios, the BLR geometry seems to be different. One possible explanation is that when the Eddington ratio is fairly low (i.e. $\lesssim 0.01$), the accretion mode may be changed from the standard optically thick and geometrically thin disk to an Advection-Dominated Accretion Flow (ADAF), or more generally, to a Radiatively Inefficient Accretion Flow (RIAF) (Sulentic et al. 2006). For example, 3C390.3 is a typical double-peaked radio galaxy with FWHM(Hβ)~ 9958 km s^{-1}. Due to its very low $L_{\rm Bol}/L_{\rm Edd} \sim 0.01$, it is suggested that the inner region of its disk is an ion-supported torus, and the double-peaked emission lines would be produced in the outer fragmented clumps which are illuminated by the inner ADAF (Czerny et al. 2004). As the Eddington ratio decreases, the source would experience changes in the structure of the accretion disk, and the RIAF tends to be increasingly dominated. In such a scenario, strong winds are unlikely to be maintained. So, wind in the BLR would be absent in highly sub-Eddington objects (e.g. Pop.B) which appear to be dominated by radiatively inefficient accretion processes.

Speculations such as whether the structure and dynamics of the BLR can be interpreted in such a scenario based on the disk and wind theory, and whether the different structures in the BLR could be responsible for the different populations of AGNs which are all connected with the Eddington ratio, will be tested by larger size samples with advantage.

5 CONCLUSIONS

The reverberation mapping technique has dramatically improved the measurement of black hole masses in active galactic nuclei. However, the uncertainties in the BH masses strongly depend on the geometry of the broad line region (characterized by the factor f), and whether the BH mass based on reverberation mapping satisfies the requirement of energy budget should be tested. We have checked the BH mass from the method based on the accretion disk model with vertical structure applied to a detailed emergent spectrum. We find that the reverberation-based masses are in agreement with masses from AD models in two thirds of the present sample while the reverberation mapping technique underestimated the black hole masses in about one third of objects. It supports the recent arguments on the possible systematic uncertainties in the reverberation mapping measurements. The geometry factor f derived provides a strong support to the disk

and wind paradigm of BLR. We find that the factors f are significantly different for high and low Eddington ratio objects. We suggest that the BLR geometry strongly depends on the Eddington ratio and that two kinds of BLR geometry may exist in AGNs, with strong wind dominant when the Eddington ratio is high enough. These results may put some constraints on the theoretical model of the BLR, and have some important implications on the reverberation-based BH mass estimates.

Acknowledgements The author is grateful to Jian-Min Wang, and thanks Rüdiger Staubert and Peter Friedrich for kindly providing the accretion disk code which achieves a self-consistent solution to vertical structure of accretion disk. The author would like to thank an anonymous referee for improving the presentation of this work. Discussions are acknowledged among the members of the AGN group in IHEP. We have made use of the NASA/IPAC Extragalactic Database (NED) which is operated by the Jet Propulsion Laboratory, California Institute of Technology, under contract with the National Aeronautics and Space Administration, observations obtained with the *XMM-Newton*, an ESA science mission, with instruments and contributions directly founded by ESA Member States and the USA(NASA), and reverberation mapping data published in *http://www.astronomy.ohio-state.edu/∼agnwatch/* as well as *http://wise-obs.tau.ac.il/∼shai/PG/*.

References

Arnaud K. A., Branduardi-Raymont G., Culhane J. L. et al., 1985, MNRAS, 217, 105
Bentz M. C., Peterson B. M., Pogge R. W. et al., 2006, ApJ, 644, 133
Blandford R. D., McKee C. F., 1982, ApJ, 255, 419
Brocksopp C., Starling R. L. C. et al., 2006, MNRAS, 366, 953
Chen K., Halpern J. P., 1989, ApJ, 344, 115
Collin S., Kawaguchi T., Peterson B. M., Vestergaard M., 2006, A&A, 456, 75
Crummy J., Fabian A. C., Gallo L., Ross R. R., 2006, MNRAS, 365, 1067
Czerny B., Rózanska A., Kuraszkiewicz J. et al., 2004, A&A, 428, 39
Denney K. D., Bentz M. C., Peterson B. M. et al., 2006, ApJ, 653, 152
Dörrer T., Riffert H., Staubert R., Ruder H., 1996, A&A, 311, 69
Dumont A. M., Collin-Suffrin S., 1990, A&A, 229, 292
Eracleous M., Halpern J. P., 1994, ApJS, 90, 1
Eracleous M., Halpern J. P., 2003, ApJ, 599, 886
Elvis M., Lockman F., Wilkes B. J., 1989, AJ, 97, 777
Fabian A. C., Vaughan S., Nandra K. et al., 2002, MNRAS, 335, L1
Goodman J., 2003, MNRAS, 339, 937
Huré J., 1998, A&A, 337, 625
Kaspi S., Maoz D., Netzer H. et al., 2005, ApJ, 629, 61
Kaspi S., Smith P. S., Netzer H. et al., 2000, ApJ, 533, 631
Kishimoto M., Antonuccci R., Blaes O., 2005, MNRAS, 364, 640
Krolik J. H., 2001, ApJ, 551, 72
Lamastra A., Matt G., Perola G. C. et al., 2006, A&A, 460, 487
Laor A., Netzer H., 1989, MNRAS, 238, 897
Laor A., 1990, MNRAS, 246, 369
Lockman F. J., Savage B. D., 1995, ApJS, 97, 1
Malkan M. A., 1988, Adv. Space Res., Vol.8, p.49
Marziani P., Zamanov R. K., Sulentic J. W. et al., 2003, MNRAS, 345, 1133
Marziani P., Dultzin-Hacyan D., Sulentic J. W., 2006, astro-ph/0606678
Murphy E. D., Lockman F., Laor A., Elvis M., 1996, ApJS, 105, 369
Murray N., Chiang J., 1997, ApJ, 474, 91
Murray N., Chiang J., 1995, ApJ, 454, 105
Murray N., Chiang J., Grossman S. A., Voit G. M., 1995, ApJ, 451, 498
Neugebauer G. et al., 1986, ApJ, 308, 815
Neugebauer G. et al., 1987, ApJS, 63, 615
Onken C. A., Ferrarese L., Merritt D. et al., 2004, ApJ, 615, 645
Perez E., Mediavilla E., Penston M. V. et al., 1988, MNRAS, 230, 353

Peterson B. M., Ferrarese L., Gilbert K. M. et al., 2004, ApJ, 613, 682
Peterson B. M., 1993, PASP, 105, 247
Piconcelli E., Jimenez-Bailón E., Guainazzi M. et al., 2005, A&A, 432, 15
Popović L. C., 2003, ApJ, 599, 140
Popović L. C., Stanić N., Kubićela A., Bon E., 2001, A&A, 367, 780
Porquet D., Reeves J. N., O'Brien P., Brinkmann W., 2004, A&A, 422, 85
Romano P., Zwitter T., Calvani M. et al., 1996, MNRAS, 279, 165
Ross R. R., Fabian A. C., 2005, MNRAS, 358, 211
Seaton M. J., 1979, MNRAS, 187, 73p
Shakura N. I., Sunyaev R. A., 1973, A&A, 24, 337
Shang Z., Brotherton M. S., Green R. F. et al., 2005, ApJ, 619, 41
Shapovalova A. I., Doroshenko V. T., Bochkarev N. G. et al., 2004, A&A, 422, 925
Strateva I. V., Strauss M. A. et al., 2003, AJ, 126, 1720
Sulentic J. W., Zwitter T., Marziani P. et al., 2000a, ApJ, 536, L5
Sulentic J. W., Marziani P., Dultzin-Hacyan D. et al., 2000b, ARA&A, 38, 521
Sulentic J. W., Marziani P., Zwitter T. et al., 1998, ApJ, 501, 54
Sun W.-H., Malkan M. A., 1989, ApJ, 346, 68
Trammell G. B., Vanden Berk D. E., Schneider D. P. et al., 2007, AJ, 133, 1780
Tremaine S., Gebhardt K., Bender R. et al., 2002, ApJ, 574, 740
Turner T. J., Pounds K. A., 1989, MNRAS, 240, 833
Vestergaard M., Wilkes B. J., Barthel P. D. et al., 2000, ApJ, 538, L103
Volonteri M., Madau P., Quataert E., Rees M., 2005, ApJ, 620, 69
Wandel A., Peterson B. M., Malkan M. A., 1999, ApJ, 526, 579
Wu X. B., Han J. L., 2001, ApJ, 561, L59
Zhang T. Z., Wu X. B., 2002, Chin. J. Astron. Astrophys. (ChJAA), 2, 487
Zheng W., Kriss G. A., Telfer R. C. et al., 1997, ApJ, 475, 469